Composite Structures 172 (2017) 45–60

Contents lists available at ScienceDirect

Composite Structures

journal homepage: www.elsevier.com/locate/compstruct

Shear deformation theory using logarithmic function for thick circular beams and analytical solution for bi-directional functionally graded circular beams

Anup Pydah *, R.C. Batra

Department of Biomedical Engineering and Mechanics, Virginia Polytechnic Institute and State University M/C 0219, Blacksburg, VA 24061, USA

ARTICLE INFO

Article history:
Received 7 February 2017
Revised 20 March 2017
Accepted 21 March 2017
Available online 23 March 2017

Keywords:
Bi-directional functionally graded materials
Circular beams
Shear deformation theory
Analytical solution
Sandwich beams

ABSTRACT

A shear deformation theory including a logarithmic function in the postulated expression for the circumferential displacement is developed for thick circular beams and is used to analytically solve static deformations of bi-directional functionally graded circular beams. The consideration of a logarithmic term is motivated by the displacement field in the analytical solution of the plane strain elasticity problem of a hollow circular cylindrical shell. The non-zero shear traction boundary conditions at the two major surfaces of the beam are *a priori* satisfied by the assumed displacement field. The material properties are assumed to vary according to exponential and power laws, respectively, in the tangential and the thickness directions. Parametric studies conducted for the variation of stresses and displacements indicate that material properties can be tailored to satisfy several structural constraints. For the bending of a sandwich beam with a bi-directionally graded core and homogeneous isotropic facesheets, it is found that the maximum interfacial bending stress, the peak interfacial shear stress and the maximum interfacial peeling stress can be reduced, respectively, by 20%, 44% and 42%.

1. Introduction

Curved beams are used in civil, mechanical and aerospace industries as part of grid stiffened floors, wind turbine blades, and as stringers and rings in wing and hull assemblies. Beams made of functionally graded materials (FGMs) have smooth material composition profiles [1] that help mitigate interface problems like delamination failure observed in layered composites [2] while also providing multi-functionalities. For example, by combining the thermal resistance of ceramics with the toughness, wear resistance and machinability of metals [3,4], FG beams can be designed with high stiffness-to-weight ratios. In this study, we develop a shear deformation theory for thick circular beams and use it to analyze static deformations of bi-directional FGM circular beams.

One way to derive a highly effective beam/plate/shell theory is to postulate displacement fields in terms of basis functions [5–8] that appear in the analytical solution of the corresponding boundary value problem solved using the linear elasticity theory. Borrowing from expressions for the tangential displacements for a hollow circular cylindrical shell subjected to surface tractions on its inner and outer surfaces, given for example in [9], we postulate an expression for the tangential displacement of a circular thick beam that includes a combination of algebraic and logarithmic functions of the radial coordinate as well as terms multiplying tangential tractions applied on the two major surfaces. The radial displacement is assumed to be a function of the angular position only. Stresses derived from the postulated displacements and Hooke's law satisfy the tangential traction boundary conditions on the two major surfaces.

Deformations for a curved beam differ from those of a straight beam in that a radial displacement of a point produces axial strain and axial stress in the circumferential direction whereas in a straight beam only displacement gradients induce strains. In the proposed beam theory, the effect of the transverse normal strain (i.e., the thickness-stretch effect) is not considered, and the transverse normal (or radial) stress is obtained by using a one-step stress recovery scheme (SRS) by integrating the equation of equilibrium in the radial direction.

The mechanics of *straight* FGM beams with material properties graded in only one direction, either through-the-thickness [4,10–17] or axially [18–21] have been extensively analyzed, with focus mostly on thickness-wise gradations. Bi-directionally graded beams wherein the material properties vary along the axis and

* Corresponding author.
E-mail addresses: anpydah@vt.edu (A. Pydah), rbatra@vt.edu (R.C. Batra).

http://dx.doi.org/10.1016/j.compstruct.2017.03.072
0263-8223/

thickness of the beam simultaneously have recently been shown to improve structural efficiency and help fulfill practical design requirements. Semi-analytical elasticity solutions based on the state space method were presented by Lu et al. [22] for the bending of bi-directional FGM straight beams while the steady-state free and forced vibration of these structures was optimized using meshless methods by Qian and Batra [23] and Goupee and Vel [24]. Simsek [25] and Wang et al. [26] studied the dynamics of bi-directional FGM straight beams using the Timoshenko and the Euler–Bernoulli beam theories, respectively. Using an exponential gradation along the beam thickness and a power law distribution along the length, an abrupt jump in natural frequencies was reported for specific values of the gradation parameters.

For curved beams, however, there is a paucity of analytical solutions for bi-directionally graded beams. Beams with material properties varied only through the thickness have been studied using the differential quadrature method [27,28], initial values method [29], variational principles [30–33], the beam theory approach [34], the power series method [35,36], the finite element method [37] and the variational iteration method [38]. Two dimensional elasticity solutions for the statics [39,40] and free vibrations [9,41,42] of FGM circular beams with thickness-wise variations in material properties have also been developed. Recently, Pydah and Sabale [43,44] presented analytical solutions for the flexure of bi-directional FGM circular beams using the Euler–Bernoulli theory and the first order shear deformation theory. However, these models were unable to capture the non-linear distribution of the transverse shear stress through the thickness of the beam and necessitated the use of a shear correction factor.

Here, we assume Young's modulus to be of the form $E(r,\theta) = E^{*}f(r)g(\theta)$ wherein $f(r)$ and $g(\theta)$ are non-dimensional functions representing the gradations along the depth (i.e., in the radial ($r-$) direction) and along the arc-length (i.e. in the tangential/axial ($\theta-$) direction). Numerical results have been computed by assuming the function $f(r)$ to be a power-law in r and $g(\theta)$ an exponential in θ. Through-the-thickness distributions of all stresses including the transverse normal stress computed using the one-step SRS are found to agree well with those from the analysis of the corresponding plane stress elasticity problems using the commercial finite element software, ABAQUS/ Standard. By decomposing the total strain energy of the beam into its components due to bending, transverse shear and transverse normal deformations, it is found that for thick circular cantilever beams (thickness/radius of the centroidal axis = 0.3) subjected to uniformly distributed loads, the strain energy due to transverse shear deformations is almost 15% of that due to bending deformations and the tip displacement is underestimated by 11% if shear deformations are not accounted for. Parametric studies conducted for the variation of the stresses and the displacements indicate that the gradation parameters can be tuned to satisfy several structural constraints. For the flexure of a sandwich beam with a bi-directional FGM core and homogeneous isotropic facesheets, significant reduction in the bending stress (20%), the shear stress (44%) and the transverse normal stress (42%) are obtained at the interface between the core and the facesheets by employing a suitably tailored bi-directional FGM core.

2. Mathematical formulation

Fig. 1 depicts a thick circular beam with radius R_0 of its centroidal axis and a rectangular cross-section of width b and thickness h. The beam subtends an arc angle θ_{tip} at the center of the fixed rectangular Cartesian coordinate axes ($\mathbf{x}_1, \mathbf{x}_2$) with the origin at point O. The beam is loaded by the applied normal tractions $q_{\text{in}}(\theta)$ and $q_{\text{out}}(\theta)$, and tangential tractions $\tau_{\text{in}}(\theta)$ and $\tau_{\text{out}}(\theta)$, respectively, on the inner and the outer surfaces of the beam (see Fig. 2 for an infinitesimal element of the beam).

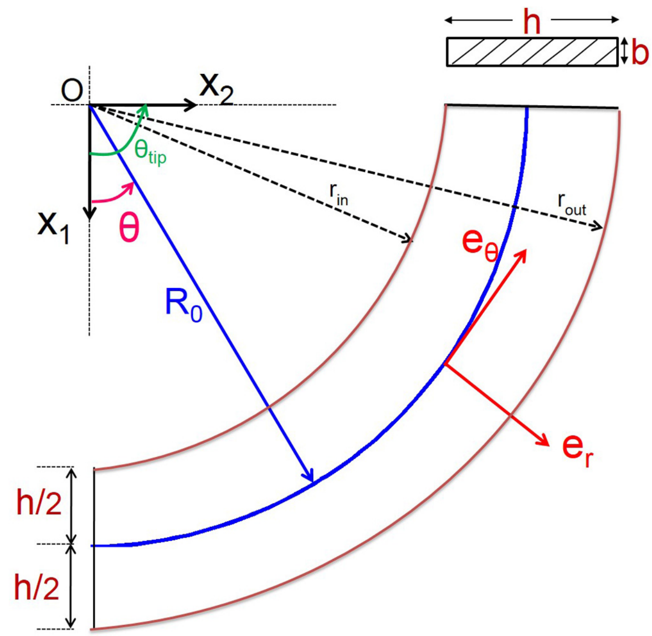

Fig. 1. Geometry of the circular beam.

2.1. Kinematics of deformation, stress resultants and equilibrium equations

The kinematics of deformation of the beam is defined using three unknown functions. Inspired by the displacement expressions for the plane strain axisymmetric deformations of a FGM cylinder derived in Ref. [9], we use a combination of algebraic and logarithmic functions of the radial coordinate, r, to define the displacement field which satisfies the tangential traction boundary conditions at the inner and the outer surfaces of the beam. The displacement components u_r (along the unit vector $\mathbf{e}_r$) and u_θ (along the unit vector $\mathbf{e}_\theta$) of an arbitrary point of the beam are assumed to be given by

$$u_r(r,\theta) = u_r^0(\theta)$$

$$u_\theta(r,\theta) = u_\theta^0(\theta) + (r - R_0)\,\phi(\theta) + U_0(r)\,\psi(\theta) + U_1(r)\,\overline{\tau_{\text{in}}} + U_2(r)\,\overline{\tau_{\text{out}}} \tag{1}$$

Here

$$\overline{\tau_{\text{in}}} = \frac{\tau_{\text{in}}(\theta)}{G(r_{\text{in}},\theta)}, \overline{\tau_{\text{out}}} = \frac{\tau_{\text{out}}(\theta)}{G(r_{\text{out}},\theta)}$$

$$\psi(\theta) = u_\theta^0 - \left(u_r^0\right)' - R_0\,\phi(\theta) \tag{2}$$

$$U_0(r) = \frac{4}{h^2}\left(r^2 - R_0^2 - 2rR_0\ln(r/R_0)\right) \tag{3}$$

$$U_1(r) = \frac{1}{h}\left(r^2 - r\,(R_0 + h/2)\,\ln(r/R_0)\right) \tag{4}$$

$$U_2(r) = \frac{1}{h}\left(r^2 - r\,(R_0 - h/2)\,\ln(r/R_0)\right) \tag{5}$$

Here, $\tau_{\text{in}}(\theta)$ and $\tau_{\text{out}}(\theta)$ are the applied tangential tractions on the inner surface ($r_{\text{in}} = R_0 - h/2$) and the outer surface

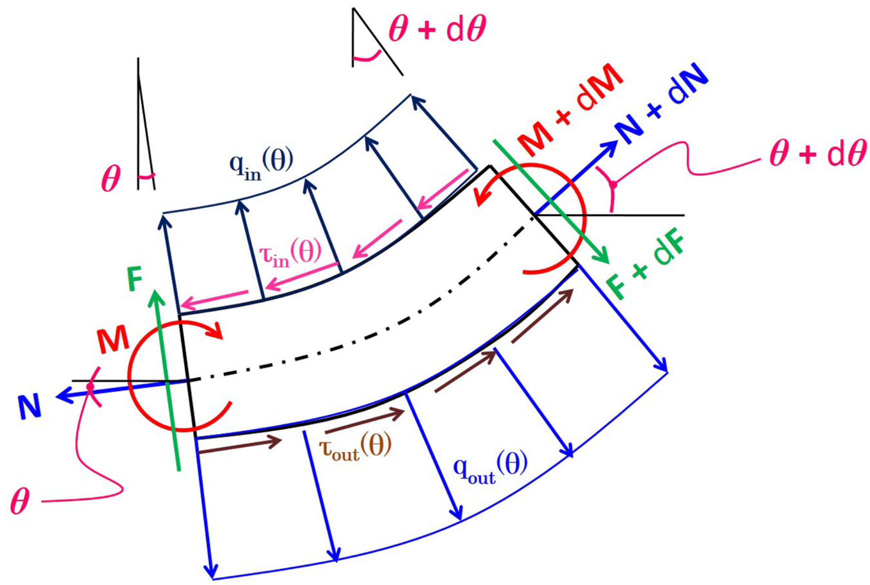

Fig. 2. Free body diagram for a beam element.

($r_{out} = R_0 + h/2$) of the beam, respectively, $u_r^0(\theta)$ is the radial displacement of a point on the centroidal axis of the cross-section, $\phi(\theta)$ is the rotation of the cross-section about the z-axis, and a prime $(.)'$ denotes differentiation with respect to θ. This beam theory neglects effects of the transverse normal strain ϵ_r (i.e., the thickness-stretch effect) on deformations of the beam. Using Eq. (1), the linear axial (tangential) bending strain $\varepsilon_\theta(r,\theta) = \frac{u_r}{r} + \frac{1}{r}\frac{\partial u_\theta}{\partial \theta}$, the transverse shear strain $\gamma_{r\theta}(r,\theta) = \frac{1}{r}\frac{\partial u_r}{\partial \theta} + \frac{\partial u_\theta}{\partial r} - \frac{u_\theta}{r}$, the axial bending stress $\sigma_\theta(r,\theta)$ and the transverse shear stress $\tau_{r\theta}(r,\theta)$ are given by

$$\varepsilon_\theta = \frac{1}{r}\left\{u_r^0 + \left(u_\theta^0\right)' + (r - R_0)\,\phi' + U_0\,\psi' + U_1\overline{\tau_{in}}' + U_2\overline{\tau_{out}}'\right\} = \frac{\sigma_\theta}{E(r,\theta)} \tag{6}$$

$$\gamma_{r\theta} = \frac{1}{h^2 r}\left(h^2 - 4(r - R_0)^2\right)\left(\left(u_r^0\right)' - u_\theta^0 + R_0\,\phi\right) - (r - R_0)\tau_{as} + \tau_s = \frac{\tau_{r\theta}}{G(r,\theta)} \tag{7}$$

where

$$\tau_s = \frac{1}{2}(\overline{\tau_{in}} + \overline{\tau_{out}}),\ \tau_{as} = \frac{1}{h}(\overline{\tau_{in}} - \overline{\tau_{out}})$$

and it has been assumed that the material is isotropic and obeys Hooke's law with Young's modulus $E(r,\theta)$ and the shear modulus $G(r,\theta)$. We have also assumed that the width $b \ll R_0$ and that a state of plane stress exists in the $r-\theta$ plane so that $\sigma_{zz} = 0$. Here the $z-$direction is perpendicular to the $r-\theta$ plane. We have not modified E to satisfy the requirement $\sigma_r = 0$ implicitly assumed in Hooke's law. The transverse normal stress σ_r is determined through a one-step SRS explained later. The three functions $u_r^0(\theta), u_\theta^0(\theta)$ and $\phi(\theta)$ are the primary unknowns in the problem. We note that the solution of the differential equation $\epsilon_\theta = 0$ need not be independent of θ. Thus, the so-called neutral axis need not be the curve $r = $ constant. Of course, results for the plane strain problem can be deduced from those of the plane stress problem by modifying E and G in the standard way.

The axial force $N(\theta)$, the bending moment $M(\theta)$ about the z-axis through the midpoint of the beam thickness and the transverse shear force $F(\theta)$ at any section are defined as

$$N(\theta) = b\int_{R_0-\frac{h}{2}}^{R_0+\frac{h}{2}} \sigma_\theta(r,\theta)\,dr$$

$$M(\theta) = b\int_{R_0-\frac{h}{2}}^{R_0+\frac{h}{2}} \sigma_\theta(r,\theta)\,(r - R_0)dr$$

$$F(\theta) = b\int_{R_0-\frac{h}{2}}^{R_0+\frac{h}{2}} \tau_{r\theta}(r,\theta)\,dr \tag{8}$$

In the Euler–Bernoulli beam theory, the location of the neutral axis is obtained by setting the resultant axial force equal to zero, for the case of pure bending. For the present beam theory, the solution of the differential equation $N(\theta) = 0$ need not be independent of θ even for a homogeneous beam.

By multiplying the following two equilibrium equations of the 2D linear elasticity

$$\frac{\partial(r\sigma_r)}{\partial r} + \frac{\partial \tau_{r\theta}}{\partial \theta} - \sigma_\theta = 0 \tag{9}$$

$$\frac{1}{r}\frac{\partial(r^2\tau_{r\theta})}{\partial r} + \frac{\partial \sigma_\theta}{\partial \theta} = 0 \tag{10}$$

by b, Eq. (10) by br, and integrating the resulting expressions across the beam thickness in the radial direction, we get the equations of equilibrium along the radial and the tangential directions, and of the moment about the z-axis.

$$F' - N + b(r_{out}q_{out} - r_{in}q_{in}) = 0$$

$$N' + F + b(r_{out}\tau_{out} - r_{in}\tau_{in}) = 0$$

$$M' - R_0F + \frac{bh}{2}(r_{out}\tau_{out} + r_{in}\tau_{in}) = 0 \tag{11}$$

We note that use of the second equation has been made in the third equation to obtain its final form. The third term appearing on the left hand side of Eq. (11) clearly indicates that the same surface traction applied on the inner and the outer surfaces will induce different deformations of the beam. In order to analyze deformations of the beam due to a normal point load P_0 on the beam inner surface at $\theta = \theta_0$, the load is considered as a normal traction q_{in} acting over an infinitesimal patch of arc length ϵ and width b such that

$$q_{\rm in} = P_0 \frac{\mathrm{H}\left(r_{\rm in}, \theta - (\theta_0 - \frac{\epsilon}{2})\right) - \mathrm{H}\left(r_{\rm in}, \theta - (\theta_0 + \frac{\epsilon}{2})\right)}{b\epsilon}$$

where $\mathrm{H}(\theta)$ is the Heaviside function and $\epsilon \ll 1$. This expression for $q_{\rm in}$ can be substituted into Eq. (11-1) of equilibrium along the radial direction, since $\sigma_r(r_{\rm in}, \theta) = q_{\rm in}$.

2.2. Gradation laws

For bi-directional FGM beams, Young's modulus $E(r,\theta)$ and the shear modulus $G(r,\theta)$ are assumed to have the following variation

$$P(r,\theta) = P^* f(r) g(\theta) \tag{12}$$

where $P(r,\theta)$ can be either $E(r,\theta)$ or $G(r,\theta)$, P^* is a constant (with dimensions $ML^{-1}T^{-2}$; M is mass, L length and T time), and $f(r)$ and $g(\theta)$ are non-dimensional functions representing gradations along the radial and the circumferential directions, respectively. Poisson's ratio ν is assumed to remain constant so that $G^* = E^*/2(1+\nu)$. As pointed out in Refs. [45,9], this assumption has a negligible effect on stresses but can noticeably affect displacements. For numerical examples in this study, we assume

$$f(r) = 1 + \left(\frac{P_{in}}{P_{out}} - 1\right)\left(\frac{1}{2} - \frac{r - R_0}{h}\right)^{\lambda_r} \quad (\text{with } P^* = P_{out}) \tag{13}$$

$$g(\theta) = \exp(\lambda_\theta \theta) \tag{14}$$

where θ is in radians and λ_r and λ_θ are non-dimensional parameters (also called *gradation indices*) dictating the gradation along the radial and the circumferential directions, respectively. P_{in} , P_{out} are defined as

$$P_{in} = P(R_0 - h/2, 0) \text{ and } \quad P_{out} = P(R_0 + h/2, 0)$$

A bi-directional gradation scheme according to Eqs. (12)–(14) is shown in Fig. 3 with $E_{in} = 380$ GPa, $E_{out} = 210$ GPa, $\lambda_r = -1$ and $\lambda_\theta = -0.25$. Note that $\lambda_r = \lambda_\theta = 0$ for a homogeneous material beam.

Using Eqs. (8) through (12), the forces and moments are found to be

$$N = bE^* g(\theta)\left\{\left[u_r^0 + (u_\theta^0)'\right]\alpha_0 + \left[(u_\theta^0)' - (u_r^0)'' - R_0\phi'\right]\alpha_1 + \phi'\alpha_2\right\} + k_1 \tag{15}$$

$$M = bE^* g(\theta)\left\{\left[u_r^0 + (u_\theta^0)'\right]\alpha_2 + \left[(u_\theta^0)' - (u_r^0)'' - R_0\phi'\right]\alpha_3 + \phi'\alpha_4\right\} + k_2 \tag{16}$$

$$F = bG^* g(\theta)\left\{\alpha_5\left((u_r^0)' - u_\theta^0 + R_0\phi\right) + \alpha_6\tau_s - \alpha_7\tau_{as}\right\} \tag{17}$$

where

$$\alpha_0 = \int_{R_0-\frac{h}{2}}^{R_0+\frac{h}{2}} \frac{f(r)}{r} dr$$

$$\alpha_1 = \frac{4}{h^2}\int_{R_0-\frac{h}{2}}^{R_0+\frac{h}{2}} \frac{f(r)\left(r^2 - R_0^2 + r(1 - 2R_0 \ln(r))\right)}{r} dr$$

$$\alpha_2 = \int_{R_0-\frac{h}{2}}^{R_0+\frac{h}{2}} \frac{f(r)(r - R_0)}{r} dr$$

$$\alpha_3 = \frac{4}{h^2}\int_{R_0-\frac{h}{2}}^{R_0+\frac{h}{2}} \frac{f(r)(r - R_0)\left(r^2 - R_0^2 + r(1 - 2R_0 \ln(r))\right)}{r} dr$$

$$\alpha_4 = \int_{R_0-\frac{h}{2}}^{R_0+\frac{h}{2}} \frac{f(r)(r - R_0)^2}{r} dr$$

$$\alpha_5 = \frac{1}{h^2}\int_{R_0-\frac{h}{2}}^{R_0+\frac{h}{2}} \frac{f(r)\left(h^2 - 4(r - R_0)^2\right)}{r} dr$$

$$\alpha_6 = \int_{R_0-\frac{h}{2}}^{R_0+\frac{h}{2}} f(r) dr$$

$$\alpha_7 = \int_{R_0-\frac{h}{2}}^{R_0+\frac{h}{2}} f(r)(r - R_0) dr \tag{18}$$

$$k_1 = bE^* g(\theta)(\overline{\tau_{\rm in}}'\beta_{10} + \overline{\tau_{\rm out}}'\beta_{20})$$

$$k_2 = bE^* g(\theta)(\overline{\tau_{\rm in}}'\beta_{11} + \overline{\tau_{\rm out}}'\beta_{21})$$

$$\beta_{ij} = \int_{R_0-\frac{h}{2}}^{R_0+\frac{h}{2}} \frac{f(r)U_i(r)(r - R_0)^j}{r} dr, \; i,j = 0,1,2.$$

For a homogeneous material ($\lambda_r = \lambda_\theta = 0$), expressions for the constants $\alpha_i (i = 0, 1, \ldots, 7)$ are given in Appendix A.

For statically determinate circular beams the stress resultants $N(\theta)$, $M(\theta)$ and $F(\theta)$ can be directly determined from equilibrium Eq. (11) and the associated boundary conditions $N(\theta_{tip}) = N^*, F(\theta_{tip}) = F^*$ and $M(\theta_{tip}) = M^*$, where N^*, F^* and M^* are the applied tip loads. Substituting for $\phi(\theta)$ from Eq. (17), Eqs. (15) and (16) are solved for $\left[u_r^0 + (u_\theta^0)'\right]$ and $\left[(u_\theta^0)' - (u_r^0)''\right]$ to get

$$u_r^0 + (u_\theta^0)' = \frac{1}{b(\alpha_2^2 - \alpha_0\alpha_4)}\left(\frac{\overline{M}\alpha_2 - \overline{N}\alpha_4}{E^* g(\theta)} + \frac{(\alpha_2\alpha_3 - \alpha_1\alpha_4)}{G^*\alpha_5}(F)'\right) \tag{19}$$

$$(u_\theta^0)' - (u_r^0)'' = \frac{1}{b(\alpha_2^2 - \alpha_0\alpha_4)}\left(\frac{\overline{N}R_0\alpha_2 - \overline{M}R_0\alpha_0}{E^* g(\theta)} + \frac{\bar{\alpha}}{G^*}\overline{F}'\right) \tag{20}$$

where

$$\overline{N} = N - k_1, \overline{M} = M - k_2$$

$$\bar{\alpha} = \frac{R_0\alpha_1\alpha_2 - R_0\alpha_0\alpha_3 + \alpha_0\alpha_4 - \alpha_2^2}{\alpha_5}$$

$$\overline{F} = \frac{F}{g(\theta)} - bG^*(\alpha_6\tau_s - \alpha_7\tau_{as})$$

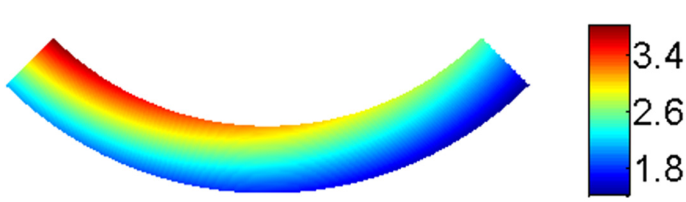

Fig. 3. Variation of E/E^* in a bi-directional FGM curved beam with $\lambda_r = 1$, $\lambda_\theta = -0.25$. The beam thickness is exaggerated for illustration.

From Eqs. (19) and (20), we get the governing differential equation for $u_r^0(\theta)$:

$$\left(u_r^0\right)'' + u_r^0 = \frac{1}{b\left(\alpha_2^2 - \alpha_0\alpha_4\right)}\left(\frac{\overline{M}\alpha_M - \overline{N}\alpha_N}{E^* g(\theta)} + \frac{\alpha_F}{G^*}\overline{F}'\right) \tag{21}$$

where

$$\alpha_M = R_0\alpha_0 + \alpha_2$$

$$\alpha_N = R_0\alpha_2 + \alpha_4$$

and

$$\alpha_F = \frac{\alpha_2^2 - R_0\alpha_1\alpha_2 + R_0\alpha_0\alpha_3 - \alpha_0\alpha_4 - \alpha_1\alpha_4 + \alpha_2\alpha_3}{\alpha_5}$$

Note that the right hand side of Eq. (21) is an explicit function of θ. Once $u_r^0(\theta)$ is determined, $u_\theta^0(\theta)$ can be obtained by integrating the first order differential Eq. (19). Finally, $\phi(\theta)$ can be determined from the algebraic Eq. (17). The solution to these two ordinary differential equations requires three additional boundary conditions to be specified at $\theta = 0$.

For a clamped edge:

$$u_r^0(0) = 0,\ u_\theta(R_0, 0) = 0 \text{ and } \left(u_r^0\right)'(0) = 0 \tag{22}$$

For a pinned edge:

$$u_r^0(0) = 0,\ u_\theta(R_0, 0) = 0 \text{ and } M(0) = 0 \tag{23}$$

For a roller that restrains the radial displacement:

$$u_r^0(0) = 0,\ N(0) = 0 \text{ and } M(0) = 0 \tag{24}$$

Hence, a total of 6 boundary conditions are required to analyze the deformation of statically determinate beams. For a statically indeterminate beam, the additional reactions are treated as unknown externally applied loads and the problem solved as above. Using the associated displacement boundary conditions at the supports, like (22)–(24), the unknown reactions are determined. For example, consider a cantilever beam with a roller support at the tip. The reaction at the roller R_F is treated as an unknown applied load on the structure and equations of equilibrium can be solved for $N(\theta), M(\theta)$ and $F(\theta)$ in terms of the applied loads and R_F. Using the boundary conditions at the clamped edge (22) and the additional condition $u_r^0(\theta_{tip}) = 0$, the governing Eq. (21) can be solved for $u_r^0(\theta)$ and R_F can be determined.

Once the bending stress σ_θ and the transverse shear stress $\tau_{r\theta}$ have been obtained from Eqs. (6) and (7), the transverse normal stress $\sigma_r(r, \theta)$ at $r = r^*$ is determined by using a one-step SRS which involves integrating the equilibrium Eq. (9) in the radial direction from $r = r_{\text{in}}$ to $r = r^*$ with the boundary condition $\sigma_r(r_{\text{in}}, \theta) = q_{\text{in}}(\theta)$. The discrepancy between $\sigma_r(r_{\text{out}}, \theta)$ and $q_{\text{out}}(\theta)$ will serve as a check on the accuracy of the solution. The procedure can be summarized as.

- Compute constants α_i $(i = 0, 1, \ldots, 7)$ using Eq. (18).
- Solve equations of equilibrium (11) for $N(\theta)$, $M(\theta)$ and $F(\theta)$ treating any indeterminate reactions as unknown applied loads.
- Solve Eq. (21) for $u_r^0(\theta)$.
- Obtain $u_\theta^0(\theta)$ by integrating Eq. (19).
- Determine $\phi(\theta)$ from Eq. (17).
- Determine the unknown reactions using displacement boundary conditions at the supports.
- Compute the bending stress σ_θ and the transverse shear stress $\tau_{r\theta}$ using Eqs. (6) and (7).
- Compute the transverse normal stress σ_r by using the one-step SRS.

The locations (r, θ) of the critical bending stress in the beam are found by simultaneously solving the following two equations:

$$\frac{\partial(\sigma_\theta(r,\theta))}{\partial r} = 0, \quad \frac{\partial(\sigma_\theta(r,\theta))}{\partial \theta} = 0$$

3. Example problems

3.1. Quarter circular beam with radial gradation of Young's modulus subjected to a tip moment M^*

Deformations of a radially graded ($\lambda_\theta = 0$) quarter circular cantilever beam with $R_0 = 0.55$ m, $h = 0.1$ m, $b = 1$ m subjected to a tip moment $M^* = 10$ kN·m. are studied and results are compared with those from the elasticity solutions of Dryden [39] and Wang and Liu [40]. The exponential gradation of Young's modulus in the thickness (radial) direction is assumed to be

$$E(r) = E_{\text{in}}\left(\frac{r}{r_{\text{in}}}\right)^2 \exp\left\{\frac{\left[\ln\left(\frac{E_{\text{out}}}{E_{\text{in}}}\right) - 2\ln\left(\frac{r_{\text{out}}}{r_{\text{in}}}\right)\right]\left[\left(\frac{r}{r_{\text{in}}}\right) - 1\right]}{\left(\frac{r_{\text{out}}}{r_{\text{in}}}\right) - 1}\right\}$$

where $E_{\text{in}} = 8.27$ GPa and $E_{\text{out}} = 5.50$ GPa. The equilibrium Eqs. (11) are solved to obtain $N = 0, F = 0$ and $M = M^*$. As a result, the through-the-thickness distribution of the bending stress σ_θ is independent of the angular position θ. Table 1 gives the distribution of the bending stress σ_θ through the beam thickness. Clearly, results from the present beam theory agree well with the elasticity solution. We note that Kardomateas [35] had solved a similar problem in 1990.

3.2. Quarter circular bi-directionally graded cantilever beam subjected to a tip shear force F^*

Unless otherwise mentioned, we set $\lambda_r = 1$, $\lambda_\theta = -0.25$, $E_{out} = E^* = 210$ GPa, $E_{in} = 380$ GPa and $\nu = 0.3$.

Deformations of a bi-directional FGM quarter circular cantilever beam ($\theta_{tip} = \pi/2$) with $R_0 = 2$ m, $h = 0.2$ m, $b = 0.1$ m and subjected to a tip shear load $F(\pi/2) = F^* = 1$ kN are studied. Integrating the ordinary differential Eq. (11) and using the boundary conditions at $\theta = \theta_{tip}$, we get

$$N = F^*\cos\theta,\ F = F^*\sin\theta \text{ and } M = -R_0F^*\cos\theta$$

From Eqs. (21), (19) and (17), displacements are determined to be

$$u_r^0(\theta) = C_{0r}\left(C_{1r}\left(e^{\lambda_\theta\theta} - 1\right)\cos\theta + \left(C_{2r} + C_{3r}e^{\lambda_\theta\theta}\right)\sin\theta\right)$$

$$u_\theta^0(\theta) = C_{0\theta}\left(\left(C_{1\theta} + C_{2\theta}e^{\lambda_\theta\theta}\right)\cos\theta + \left(C_{3\theta} + C_{4\theta}e^{\lambda_\theta\theta}\right)\sin\theta + C_{5\theta}e^{\lambda_\theta\theta}\right)$$

$$\phi(\theta) = C_{0\phi}\left(C_{1\phi}\left(e^{\lambda_\theta\theta} - \cos\theta\right) + C_{2\phi}\sin\theta\right) \tag{25}$$

where constants $C_{ir}\,(i = 0, 1, 2, 3), C_{j\theta}\,(j = 0, 1, 2, 3, 4, 5)$ and $C_{k\phi}\,(k = 0, 1, 2)$ are given in Appendix B.

Table 1
Through-the-thickness distribution of the bending stress σ_θ for a quarter circular cantilever loaded with a tip moment.

	σ_θ (MPa)		% Error
r (m)	Present Study	Dryden [39] and Wang and Liu [40]	
0.50	−7.2786	−7.2878	−0.12
0.52	−3.6102	−3.6092	0.03
0.54	−0.6539	−0.6528	0.17
0.56	1.6919	1.6911	0.05
0.58	3.5191	3.5185	0.02
0.60	4.9089	4.9132	−0.09

For comparison with the solution of the linear elasticity equations, we analyze the beam as a plane stress problem (in the $r\theta$-plane) by the finite element method (FEM) using the commercial software ABAQUS/ Standard. The beam is meshed using 8-node plane stress quadrilateral elements with reduced integration (element type CPS8R) and the load is applied as a point force at $(R_0, \pi/2)$. The bi-directional gradation was implemented in ABAQUS as an isotropic material with a user-defined USDFLD subroutine to evaluate material properties at the Gauss integration points, as detailed in Ref. [46]. A uniform 15×100 FE mesh was found to give the converged displacement and stress results within a tolerance of 0.25%. From the FE results, the work done by the applied load was calculated as 0.185 J and was found to equal the elastic strain energy ensuring that no energy was dissipated due to hour glass modes that could ensue because of the reduced integration used.

Fig. 4 shows the comparison of the centroidal displacements u_r^0 and $u_\theta(R_0, \theta)$ along the arc-length, as obtained from the FE solution and the beam theory equations. The maximum difference in displacements occurs at the tip and is found to be -0.72% for $u_r^0(\pi/2)$ and -0.82% for $u_\theta(R_0, \pi/2)$ clearly indicating the accuracy of the present beam theory.

Fig. 5 shows the comparison of the through-the-thickness distributions of the bending stress σ_θ, the transverse shear stress $\tau_{r\theta}$ and the transverse normal stress σ_r at $\theta = \pi/4$ obtained from the two analyses. The beam theory coupled with the one-step SRS accurately predicts these stresses, as well as their non-linear distributions through the beam thickness. Note that $\sigma_\theta = 0$ at $\frac{r-R_0}{h} = -0.05$.

Fig. 6 shows the comparison of the bending stress σ_θ along the arc-length on the inner surface $(r = R_0 - h/2)$ of the beam as obtained from the two approaches. The results agree well except for a discrepancy near the root, $\theta = 0$, which can be attributed to the difference in the application of the fixity boundary conditions in the two analyses. For the beam formulation, the clamped edge conditions are given by Eq. (22), while for the FE simulation, $u_r(r, 0) = 0$ and $u_\theta(r, 0) = 0$. As expected, the difference between the results for the two boundary conditions at $\theta = 0$ decays rapidly with distance from the root, as implied by the St.-Venant principle [47]. The reader is referred to Ref. [50] for a mathematical description of the St. Venant principle, and to Ref. [51] for an inhomogeneous linearly elastic helical spring. In order to model the fixity conditions similar to those specified in Eq. (22) in the FE simulation, the boundary conditions at the tip are modified to $u_r(R_0, 0) = 0$ and $u_\theta(R_0, 0) = 0$ and the bending stress results are depicted in Fig. 6. It is clear that there is no bending stress concentration observed at the root and the FE results compare well with those from the beam theory.

To study effects of the manner of application of the tip load in the FE simulations, Fig. 7 shows the through-the-thickness distribution of the transverse shear stress $\tau_{r\theta}$ close to the tip (at $\theta = 89$ deg) for three statically equivalent tip shear loads: as a point force at $r = R_0$, as a uniform tangential traction and as a tangential traction with a parabolic distribution along the beam thickness. Clearly, the way the tip load is applied affects the stress distribution near the tip with all results for $\tau_{r\theta}$ closely following a parabolic distribution through the beam thickness.

3.3. Quarter circular sandwich beam with a FGM core subjected to a tip shear force F^*

We consider a clamped circular sandwich beam with $R_0 = 2$ m consisting of a FGM core of thickness $h_c = 0.18$ m sandwiched between two homogeneous isotropic facesheets of thickness $h_f = 0.01$ m (see Fig. 8). The inner facesheet $R_0 - h_c/2 - h_f \leqslant r \leqslant R_0 - h_c/2$ has Young's modulus $E_{in} = 380$ GPa while the outer facesheet $R_0 + h_c/2 \leqslant r \leqslant R_0 + h_c/2 + h_f$ has Young's modulus $E_{out} = 210$ GPa. Poisson's ratio $\nu = 0.3$ for the facesheets and the core. At $\theta = \pi/2$, the sandwich beam is subjected to a tangential traction with resultant force $F^*(\pi/2) = 1$ kN. The analytical solution of this problem with the beam theory is similar to the one given in Eq. (25) except that the values of constants α_i $(i = 0, 1, \ldots, 7)$ are different. A uniform 40×160 FE mesh using the CPS8R elements was used to compute the converged displacement and stress results within a tolerance of 0.25% in ABAQUS.

In Fig. 9 we have compared the centroidal displacements u_r^0 and $u_\theta(R_0, \theta)$ along the arc-length while Fig. 10 shows the comparison of the through-the-thickness distributions of the bending stress

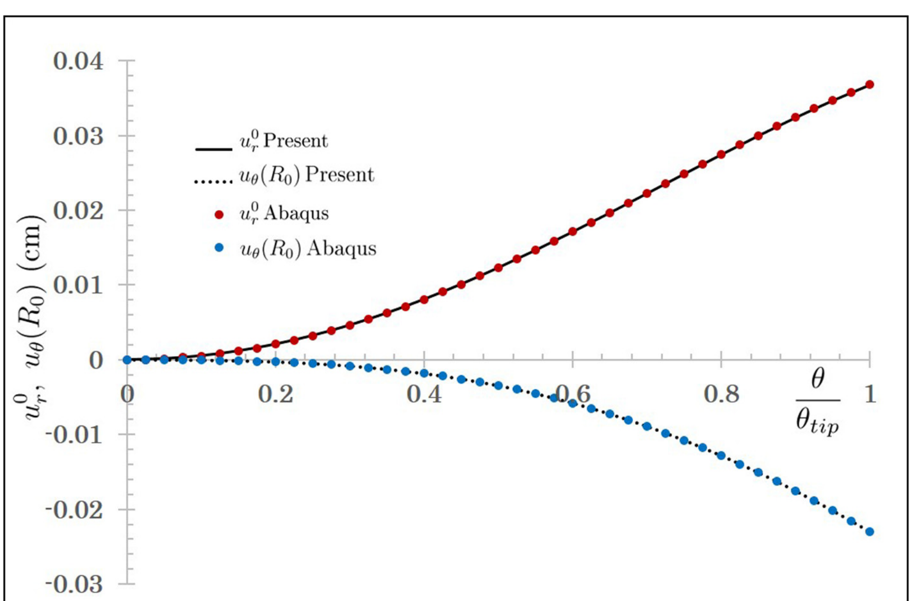

Fig. 4. Comparison of the centroidal radial $u_r^0(\theta)$ and tangential $u_\theta(R_0, \theta)$ displacements along the arc-length in the bi-directionally graded quarter circular cantilever beam subjected to a tip shear load of 1 kN.

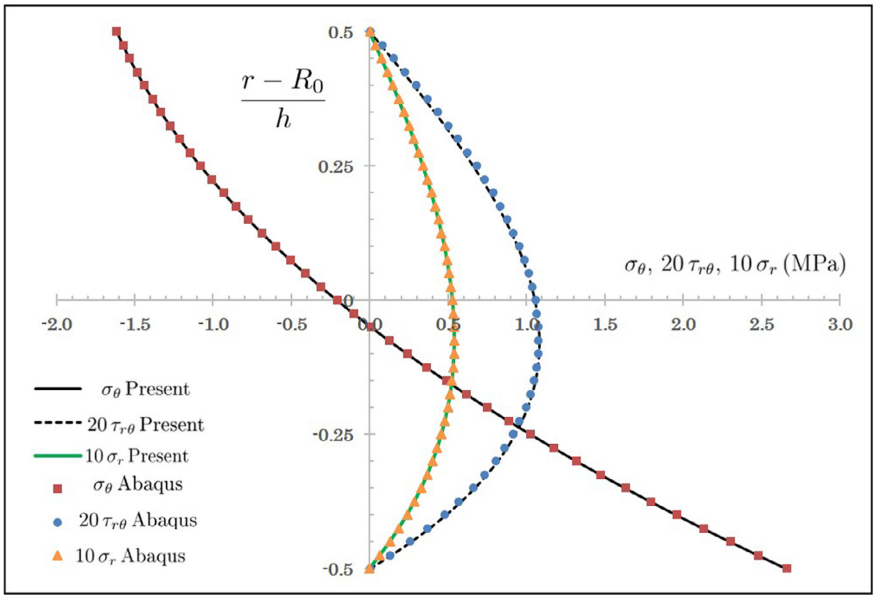

Fig. 5. Comparison of the through-the-thickness distributions of the bending stress σ_θ, the transverse shear stress $\tau_{r\theta}$ and the transverse normal stress σ_r at $\theta = \pi/4$ in the bi-directionally graded quarter circular cantilever beam subjected to a tip shear force of 1 kN.

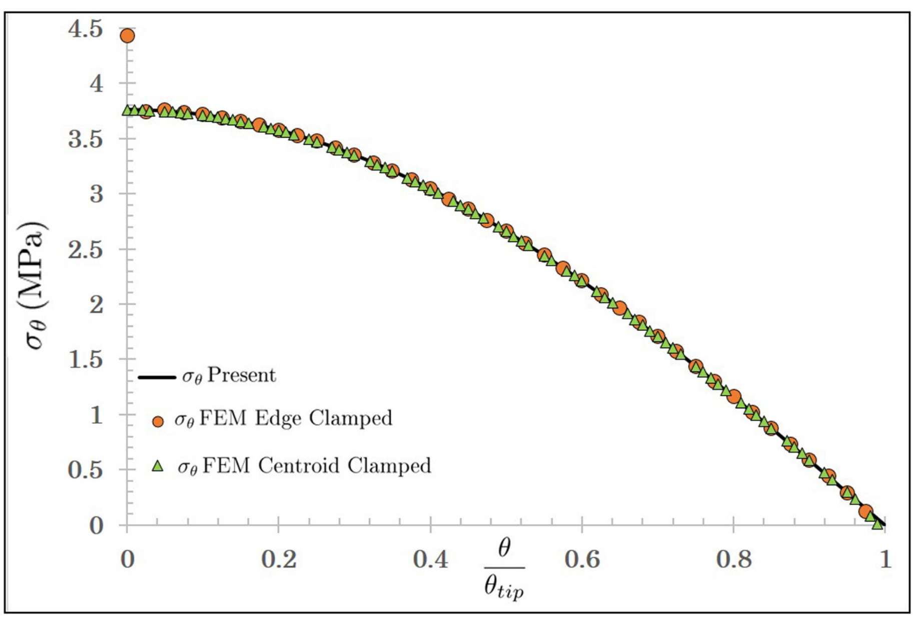

Fig. 6. Comparison of the bending stress σ_θ along the arc-length on the inner surface ($r = R_0 - h/2$) of the bi-directionally graded quarter circular cantilever beam subjected to a tip shear force of 1 kN. The FE results for the clamped condition specified by $u_r(r,0) = 0$ and $u_\theta(r,0) = 0$ are shown in orange color while those for the relaxed fixity boundary condition specified by $u_r(R_0,0) = 0$ and $u_\theta(R_0,0) = 0$ are shown in green. (For interpretation of the references to color in this figure caption, the reader is referred to the web version of this article.)

σ_θ, the transverse shear stress $\tau_{r\theta}$ and the transverse normal stress σ_r at $\theta = \pi/4$, obtained from the two analyses. The present single-layer beam theory captures well the centroidal displacements with a maximum difference of −0.41% for u_r^0 and −0.38% for $u_\theta(R_0)$ at the tip, as well as through-the-thickness non-linear distributions of the bending stress σ_θ, shear stress $\tau_{r\theta}$ and transverse normal stress σ_r (computed using the SRS for the beam theory). An accurate estimate of the interfacial stresses is needed to choose an appropriate adhesive with the requisite bond strength to prevent delamination failure at the interfaces.

3.4. Difference in results from the present and the Euler–Bernoulli beam theories

We analyze deformations of a quarter circular cantilever beam with $R_0 = 2$ m and $b = 1$ cm subjected to a uniformly distributed radial force $q^* = 5$ kN/m applied on the inner surface of the beam using the two theories. For the Euler–Bernoulli beam theory [43], the expression for u_θ in Eq. (1) has only the first two terms with $\phi = \frac{1}{R_0}\left(u_\theta^0 - (u_r^0)'\right)$.

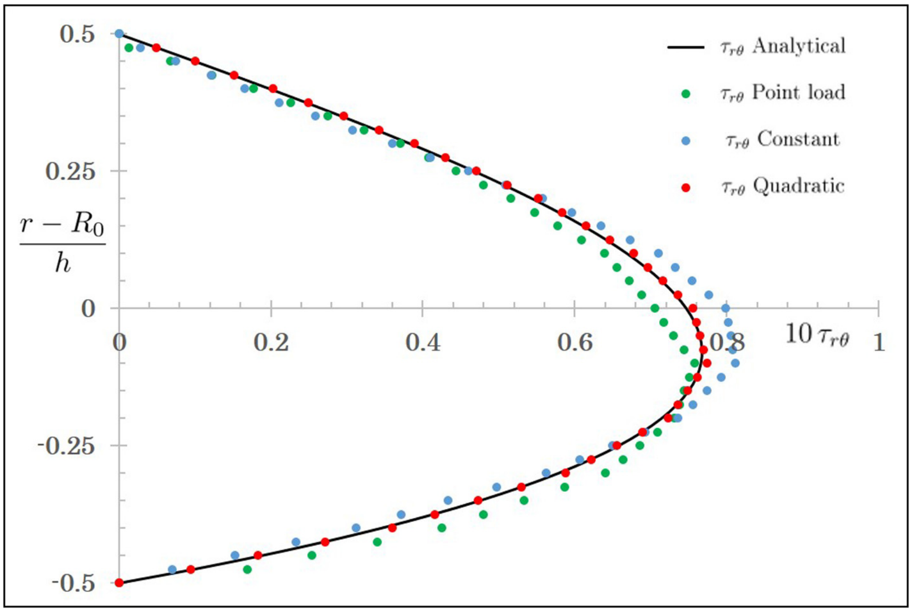

Fig. 7. Comparison of the FE results of the through-the-thickness distribution of the transverse shear stress $\tau_{r\theta}$ near the tip at $\theta = 89$ deg in the bi-directionally graded quarter circular cantilever beam subjected to three statically equivalent tip shear loads.

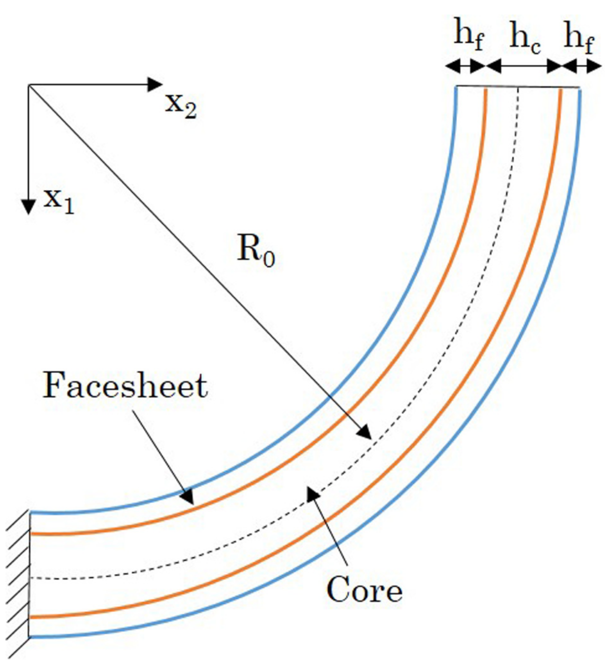

Fig. 8. Geometry of a circular sandwich beam.

We decompose the total elastic strain energy of the beam (which is equal to the work done by the applied loads) into its components due to bending, shear and transverse normal deformations as

$$U_{\text{total}} = U_{\text{bending}} + U_{\text{shear}} + U_{\text{transnormal}}$$

$$U_{\text{bending}} = \frac{1}{2} b \int_0^{\theta_{tip}} \int_{R_0-\frac{h}{2}}^{R_0+\frac{h}{2}} \sigma_\theta(r,\theta)\varepsilon_\theta(r,\theta)\, r dr\, d\theta$$

$$U_{\text{shear}} = \frac{1}{2} b \int_0^{\theta_{tip}} \int_{R_0-\frac{h}{2}}^{R_0+\frac{h}{2}} \tau_{r\theta}(r,\theta)\gamma_{r\theta}(r,\theta)\, r dr\, d\theta$$

$$U_{\text{transnormal}} = \frac{1}{2} b \int_0^{\theta_{tip}} \int_{R_0-\frac{h}{2}}^{R_0+\frac{h}{2}} \frac{\sigma_r^2(r,\theta)}{E(r,\theta)}\, r dr\, d\theta$$

Fig. 11 depicts the variation of the percentage difference in the tip displacement u_r^0, defined as $\frac{u_r^0|_{\text{EB}} - u_r^0|_{\text{Present}}}{u_r^0|_{\text{Present}}} * 100$, as the thickness h of the beam is increased, for various values of the gradation parameters. Fig. 12 shows variation of the shear energy component, normalized by the bending energy, $U_{\text{shear}}/U_{\text{bending}}$, with the beam thickness for various values of the gradation parameters. Results for a homogeneous beam ($\lambda_r = \lambda_\theta = 0$) are also shown. Clearly, as the beam thickness increases, effects of shear deformations become important, particularly for FGM beams, as indicated by the 11% difference in the tip displacement u_r^0 and the shear energy being 15% of the bending energy for $h/R_0 = 0.3$. For the assumed functional variations of the material properties, it is observed that the tangential gradation parameter λ_θ has a greater influence on the shear deformation than the radial gradation parameter λ_r. This can be explained by examining the right hand side of Eq. (21), which for $g(\theta)$ specified in Eq. (14) and with $\tau_{\text{in}} = \tau_{\text{out}} = 0$ becomes

$$(u_r^0)'' + u_r^0 = \frac{1}{e^{\lambda_\theta \theta} b(\alpha_2^2 - \alpha_0\alpha_4)} \left(\frac{M\alpha_M - N\alpha_N}{E^*} + \underline{\frac{\alpha_F}{G^*}(F' - \lambda_\theta F)} \right) \quad (26)$$

Thus λ_θ scales the value of the centroidal displacement u_r^0 determined from the particular integral of the equation. Furthermore, as λ_θ takes larger negative values, the contribution of the underlined term on the right hand side of the equation, which adds to the shear deformation in the beam, increases. Hence, the percentage difference in the tip displacement between the two beam theories would increase.

3.5. Effect of the material gradation parameters

For various values of the gradation parameters, we present numerical results for the centroidal displacements $u_r^0(\theta)$, $u_\theta(R_0, \theta)$, the bending stress σ_θ, the transverse shear stress $\tau_{r\theta}$ and the transverse normal stress σ_r for statically determinate circular beams with $R_0 = 2$ m, $h = 0.2$ m and $b = 0.1$ m for three different loads (see Fig. 2 for positive directions of the loads).

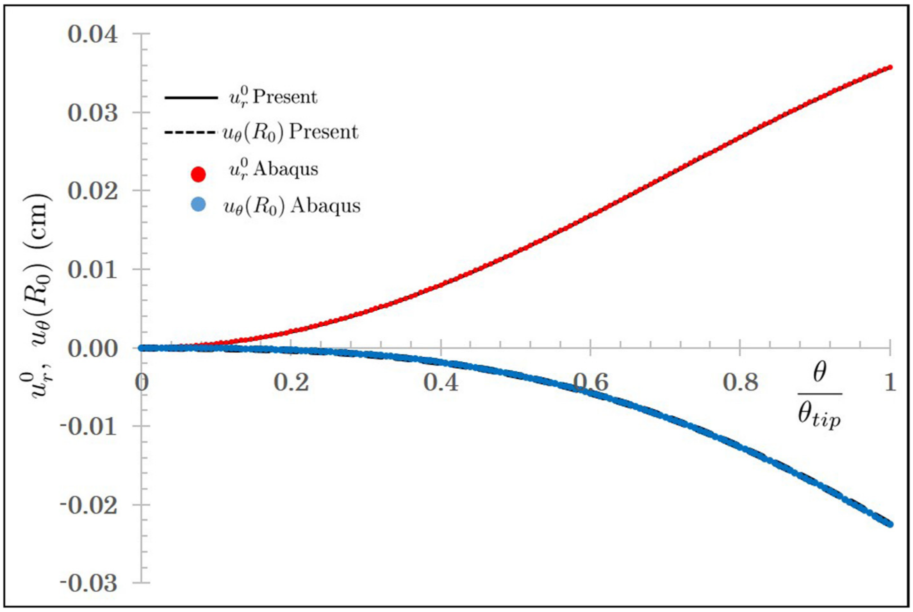

Fig. 9. Comparison of the centroidal radial $u_r^0(\theta)$ and tangential $u_\theta(R_0, \theta)$ displacements along the arc-length in the quarter circular sandwich cantilever beam subjected to a tip shear force of 1 kN.

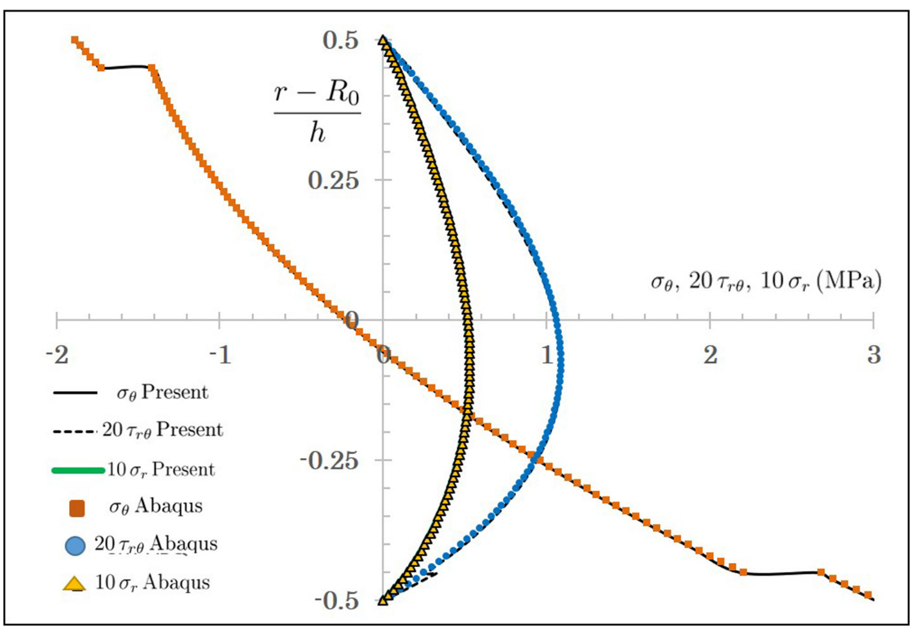

Fig. 10. Comparison of the through-the-thickness distributions of the bending stress σ_θ, the transverse shear stress $\tau_{r\theta}$ and the transverse normal stress σ_r at $\theta = \pi/4$ in the quarter circular sandwich cantilever beam subjected to a tip shear force of 1 kN.

3.5.1. Cantilever beam with a tip shear force F^*

The stress resultants determined from Eq. (11) are given by

$$N(\theta) = F^*(\sin\theta_{tip}\cos\theta - \cos\theta_{tip}\sin\theta)$$
$$F(\theta) = F^*(\sin\theta_{tip}\sin\theta + \cos\theta_{tip}\cos\theta)$$
$$M(\theta) = -R_0F^*(\sin\theta_{tip}\cos\theta - \cos\theta_{tip}\sin\theta)$$

For $\theta_{tip} = \pi/2$ and $F^* = 50$ kN, Fig. 13 and Fig. 14 show the variation of the centroidal displacements and the stresses along the arc-length and through the beam thickness.

3.5.2. Cantilever beam with a tip axial force N^*

The stress resultants are given by

$$N(\theta) = N^*(\cos\theta_{tip}\cos\theta + \sin\theta_{tip}\sin\theta)$$
$$F(\theta) = N^*(\cos\theta_{tip}\sin\theta - \sin\theta_{tip}\cos\theta)$$
$$M(\theta) = R_0N^*(1 - \cos\theta_{tip}\cos\theta - \sin\theta_{tip}\sin\theta)$$

For $\theta_{tip} = \pi/2$ and $N^* = 50$ kN, Fig. 15 shows the variation of the centroidal displacement and the stresses along the arc-length and through the beam thickness.

3.5.3. Simply-supported beam loaded with a uniformly distributed radial force q^* applied on the inner surface

The stress resultants are found to be

$$N(\theta) = -\mathscr{A}\cos\theta - \mathscr{B}\sin\theta + \mathscr{A}$$

$$F(\theta) = -\mathscr{A}\sin\theta + \mathscr{B}\cos\theta$$

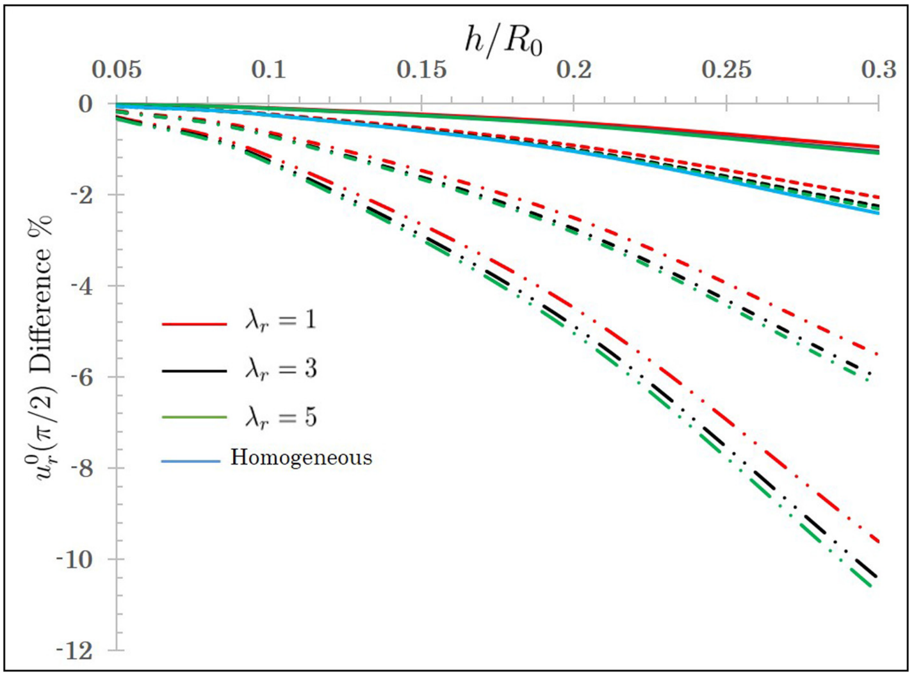

Fig. 11. Percentage difference in the tip displacement $u_r^0(\pi/2)$ from the two beam theories for $\lambda_\theta = -0.5$ (solid lines), $\lambda_\theta = -1.5$ (dashed lines), $\lambda_\theta = -2.5$ (dash-dot lines), $\lambda_\theta = -3.0$ (dash-dot-dot lines) and homogeneous ($\lambda_r = \lambda_\theta = 0$), for a quarter circular cantilever beam subjected to a uniformly distributed radial force q^* as the beam thickness h is varied from 0.1 m to 0.6 m and $R_0 = 2$ m.

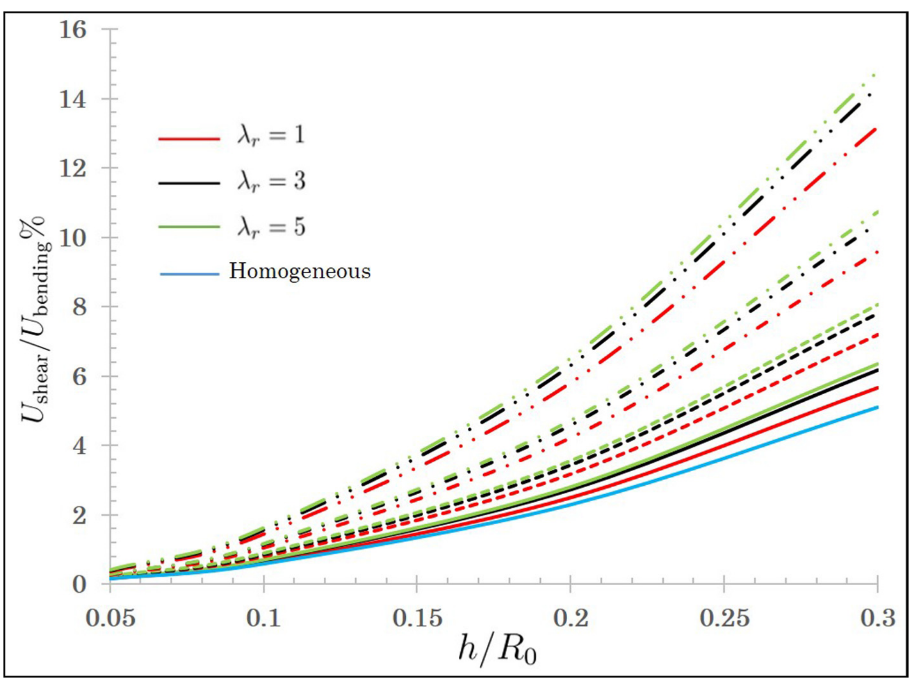

Fig. 12. Shear strain energy to bending strain energy ratio in % for $\lambda_\theta = -0.5$ (solid lines), $\lambda_\theta = -1.5$ (dashed lines), $\lambda_\theta = -2.5$ (dash-dot lines), $\lambda_\theta = -3.0$ (dash-dot-dot lines) and homogeneous ($\lambda_r = \lambda_\theta = 0$), for a quarter circular cantilever beam subjected to a uniformly distributed radial force q^* as the beam thickness h is varied from 0.1 m to 0.6 m and $R_0 = 2$ m.

$$M(\theta) = R_0(\mathscr{A}\cos\theta + \mathscr{B}\sin\theta - \mathscr{A})$$

where $\mathscr{A} = r_{\text{in}} q^*$

$$\mathscr{B} = r_{\text{in}} q^* \left(\frac{1-\cos\theta_{tip}}{\sin\theta_{tip}}\right)$$

For $\theta_{tip} = \pi/2$ and a uniformly distributed radial force $q^* = 5$ kN/m, Fig. 16 shows the variation of the centroidal displacements and the stresses along the arc-length and through the beam thickness.

From these results, the following observations are made:

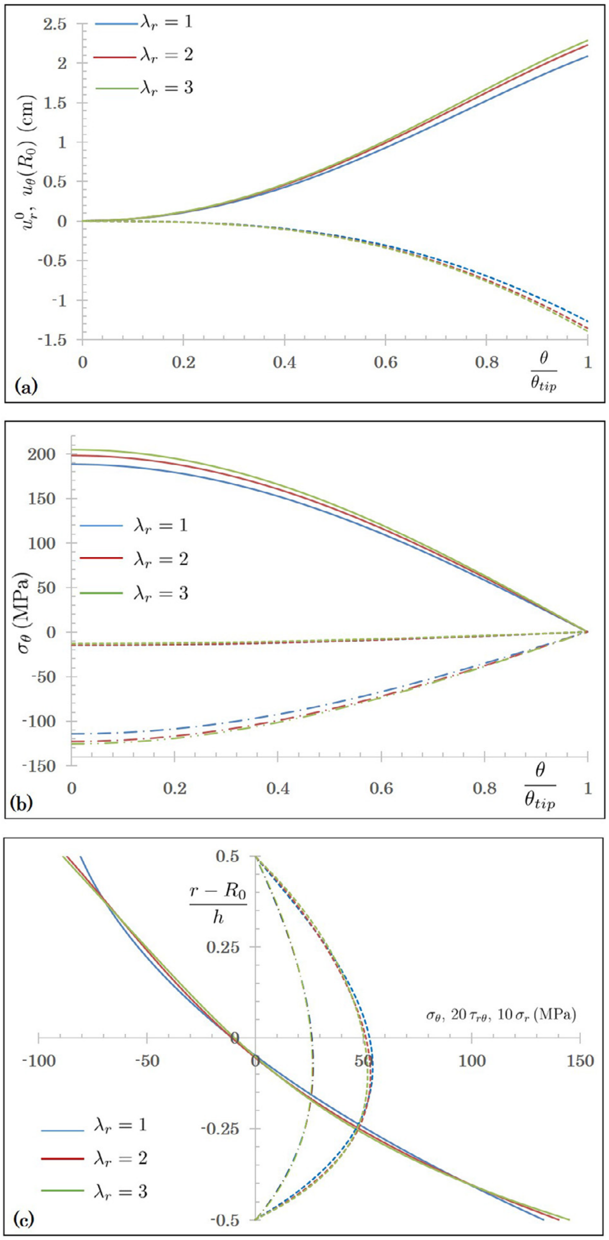

$\lambda_\theta = -0.5,\ \lambda_r = \{1, 2, 3\}$

Fig. 13. In a quarter circular cantilever beam under tip shear force $F^* = 50$ kN for $\lambda_\theta = -0.5$, $\lambda_r = \{1,\ 2,\ 3\}$ (a): Centroidal displacements u_r^0 (solid lines) and $u_\theta(R_0, \theta)$ (dashed lines); (b): Bending stress σ_θ along the arc-length at $r = R_0 - \frac{h}{2}$ (solid lines), $r = R_0$ (dashed lines) and $r = R_0 + \frac{h}{2}$ (dash-dot lines) and, (c): Bending stress σ_θ (solid lines), shear stress $20\,\tau_{r\theta}$ (dashed lines) and transverse normal stress $10\,\sigma_r$ (dash-dot lines) through the thickness at $\theta = \frac{\pi}{4}$.

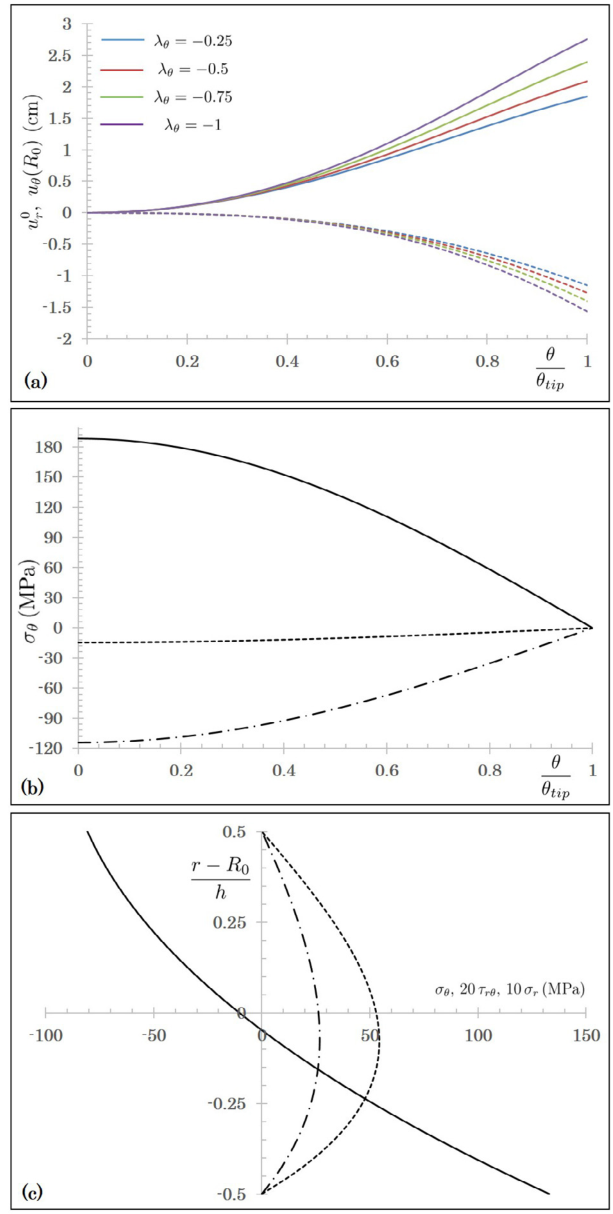

$\lambda_r = 1,\ \lambda_\theta = -\{0.25, 0.5, 0.75, 1\}$

Fig. 14. In a quarter circular cantilever beam under tip shear force $F^* = 50$ kN for $\lambda_r = 1$, $\lambda_\theta = -\{0.25,\ 0.5,\ 0.75,\ 1\}$ (a): Centroidal displacements u_r^0 (solid lines) and $u_\theta(R_0, \theta)$ (dashed lines); (b): Bending stress σ_θ along the arc-length at $r = R_0 - \frac{h}{2}$ (solid lines), $r = R_0$ (dashed lines) and $r = R_0 + \frac{h}{2}$ (dash-dot lines), and (c): Bending stress σ_θ (solid lines), shear stress $20\,\tau_{r\theta}$ (dashed lines) and transverse normal stress $10\,\sigma_r$ (dash-dot lines) through the thickness at $\theta = \frac{\pi}{4}$.

1. By choosing various values of the gradation parameters, while maintaining a constant value of Young's moduli at the inner and the outer surfaces of the beam, significant variations in the displacements $u_r^0(\theta)$ and $u_\theta(\theta)$ occur indicating the capability of the bi-directional FGM beams to be tailored to fit a wide range of structural constraints. In particular, displacements are more sensitive to the tangential gradation parameter λ_θ than to the radial gradation parameter λ_r, as can be seen from 13a, 14a, 15a,b and 16a,b.
2. As can be seen in Figs. 13c, 15d and 16d, the through-the-thickness variations of the bending stress σ_θ and the transverse shear stress $\tau_{r\theta}$ are non-linear. The transverse normal stress σ_r determined using the one-step SRS equals the applied tractions on the major surfaces of the beam (see Fig. 16d). Furthermore, irrespective of whether the bending stress at the inner surface of the beam (at $r = R_0 - h/2$) is tensile or compressive, as determined by the loading conditions and the gradation of the material properties, the centroidal axis experiences a non-zero bending stress.

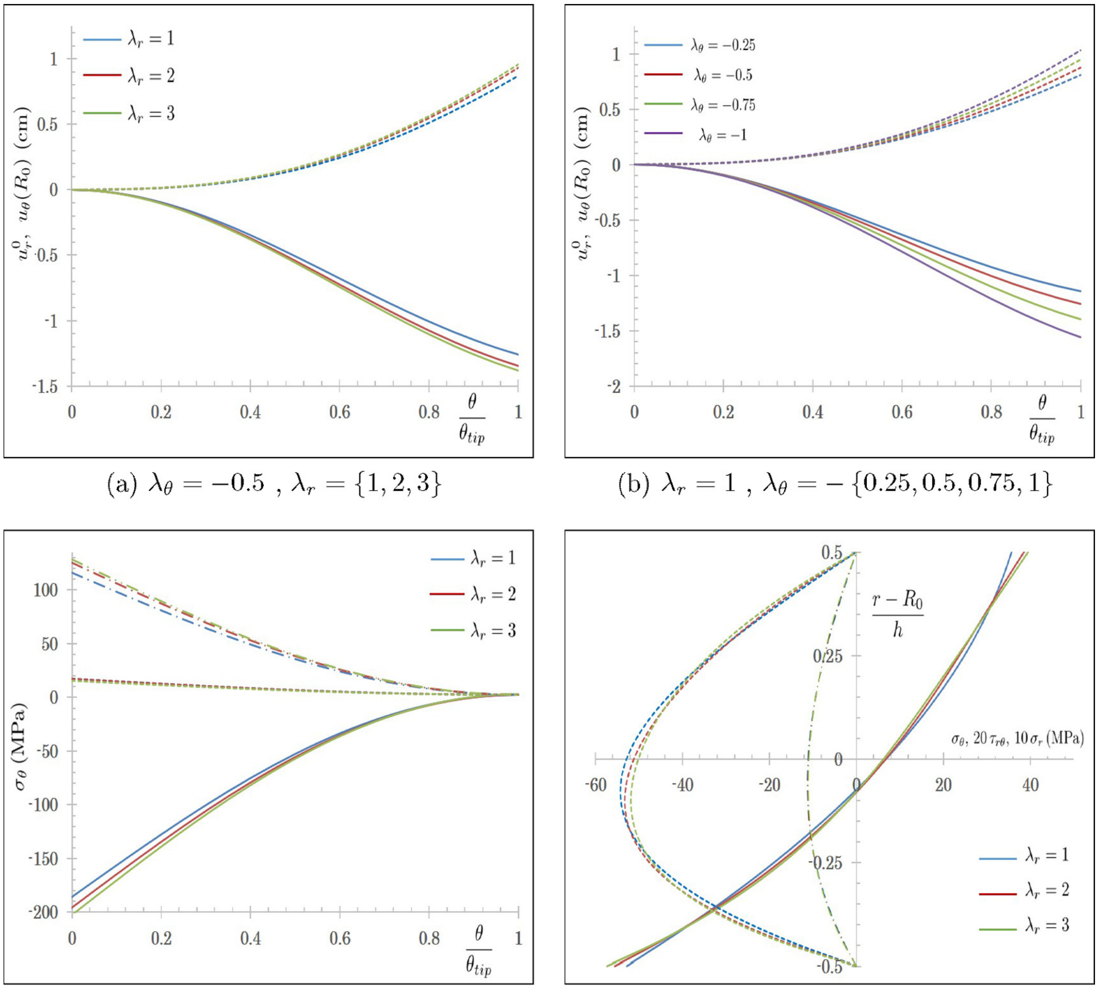

(c) $\lambda_\theta = -0.5$, $\lambda_r = \{1, 2, 3\}$ (d) $\lambda_\theta = -0.5$, $\lambda_r = \{1, 2, 3\}$

Fig. 15. In a quarter circular cantilever beam under tip axial force $N^* = 50$ kN (a), (b): Centroidal displacements u_r^0 (solid lines) and $u_\theta(R_0, \theta)$ (dashed lines); (c): Bending stress σ_θ along the arc-length at $r = R_0 - \frac{h}{2}$ (solid lines), $r = R_0$ (dashed lines) and $r = R_0 + \frac{h}{2}$ (dash-dot lines), and (d): Bending stress σ_θ (solid lines), shear stress $20\,\tau_{r\theta}$ (dashed lines) and transverse normal stress $10\,\sigma_r$ (dash-dot lines) through the thickness at $\theta = \frac{\pi}{4}$.

3. The three stresses do not depend on the tangential gradation parameter λ_θ for statically determinate beams, as can be seen in Fig. 14b, c. However, the maximum values of the bending stress (at the inner and the outer surfaces of the beam) are affected by λ_r (see Figs. 13c, 14c, 15d and 16d. This feature can be exploited by first choosing a large value of λ_θ to reduce deflections in the beams independently of the stresses, and then lowering the maximum bending stress in the beam by choosing a smaller value of λ_r.

3.6. Sandwich beams with a bi-directional FGM core

We consider a circular sandwich beam consisting of a bi-directional FGM core of thickness h_c sandwiched between two homogeneous isotropic facesheets of thickness h_f and Young's modulus E_f^0 (see Fig. 8). Young's modulus $E_c(r, \theta)$ of the core is assumed to have the following symmetric variation about the mid-line $r = R_0$ of the core:

$$E_c(r,\theta) = E_c^0\left(1 + \left(\frac{E_f^0}{E_c^0} - 1\right)\left(2\,\frac{r - R_0}{h_c}\right)^{2\lambda_r}\right)\exp\left(\lambda_\theta\theta\right) \tag{27}$$

Here E_c^0 is the value of Young's modulus at the core center. Poisson's ratio ν is assumed to remain constant in the facesheets and the core so that $G_c = E_c/2(1+\nu)$. In Fig. 17, using the single-layer theory, we present numerical results for the quarter circular cantilever sandwich beam with $R_0 = 2$ m, $h_c = 0.18$ m and $h_f = 0.01$m, subjected to a uniformly distributed radial force $q^* = 5$ kN/m on the inner surface of the beam. We set in Eq. (27), $E_f = 300$ GPa, $E_c = 30$ GPa and $\nu = 0.3$. From these results, the following observations on the versatility of using bi-directionally graded cores in circular sandwich beams are noted:

1. The tangential gradation parameter λ_θ in the core can be tuned to significantly reduce the centroidal displacements while not affecting stresses in the sandwich beam, as can be seen in Fig. 17b. For example, changing the value of λ_θ from -1 to -0.25 lowers the tip centroidal deflection u_r^0 by 26% when $\lambda_r = 1$. Furthermore, choosing a lower value of the radial gradation parameter λ_r lowers the bending stresses along the arc length of the beam while simultaneously reducing displacements in the beam (see Figs. 17a, c).
2. Significant reduction in the interfacial values of the stresses can be achieved by suitably tailoring the FGM core, as can be seen in Fig. 17d. For example, by reducing the value of λ_r from 3 to 1 in the core, the bending stress σ_θ at the interface is reduced by

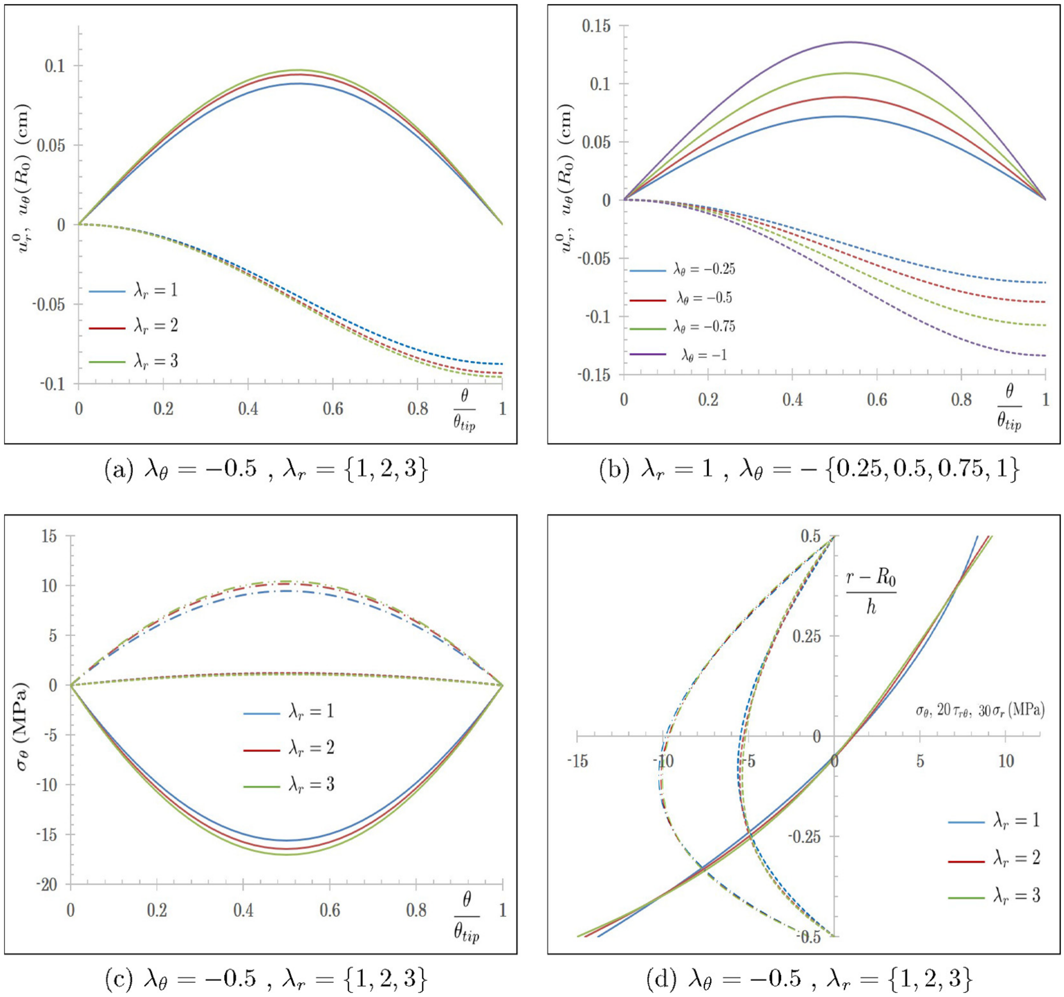

Fig. 16. In a quarter circular simply-supported beam under a uniformly distributed radial force $q^* = 5$ kN/m acting on the inner surface (a), (b): Centroidal displacements u_r^0 (solid lines) and $u_\theta(R_0, \theta)$ (dashed lines); (c): Bending stress σ_θ along the arc-length at $r = R_0 - \frac{h}{2}$ (solid lines), $r = R_0$ (dashed lines) and $r = R_0 + \frac{h}{2}$ (dash-dot lines), and (d): Bending stress σ_θ (solid lines), shear stress $20\,\tau_{r\theta}$ (dashed lines) and transverse normal stress $30\,\sigma_r$ (dash-dot lines) through the thickness at $\theta = \frac{\pi}{4}$ (dashed lines).

20%, the interfacial shear stress $\tau_{r\theta}$ by 44% and the interfacial transverse normal stress by 42% for $\lambda_\theta = -0.5$. Thus, suitable gradation of the core material can help fully utilize the core material (by allowing it to carry higher shear stresses) while maintaining low interface peeling stress (σ_r) and shear stress values to prevent delamination failure.

4. Remarks

We note that Batra and Xiao [48,49] developed a third-order shear and normal deformable theory for curved laminated beams with spatially varying curvature, e.g., beam in the form of a full sine curve, considered all geometric nonlinearities for a St. Venant – Kirchhoff beam and studied its buckling and post-buckling deformations. They found that for a beam loaded by a uniformly distributed pressure, the consideration of nonlinear effects increased the maximum stress by a factor of 4 and the maximum deflection by 1.5 over that determined using the linear theory.

5. Conclusions

Motivated by the expression for the tangential displacement field in a circular cylinder subjected to surface tractions on its inner and outer surfaces, we have developed a beam theory for thick circular beams by including a combination of an algebraic and logarithmic term in the radial coordinate in the expression for the tangential displacement postulated for the beam. Stresses derived from the hypothesized displacements exactly satisfy tangential traction boundary conditions prescribed on the major surfaces of the beam. The beam theory has been used to analyze problems for bi-directionally graded beams with Young's moduli in the radial and the circumferential directions given, respectively, by a power-law and an exponential relation of the pertinent coordinate. For five example problems studied in the paper, the beam theory stresses and displacements agree very well with those obtained by solving the corresponding plane stress problems using the linear elasticity theory and the commercial finite element software, ABAQUS/ Standard. The through-the-thickness variation of all stresses including the transverse normal stress computed using the one-step stress recovery scheme agrees well with that from the linear elasticity theory solution. The gradation in the circumferential direction only affects displacements but that in the radial direction affects the maximum values of stresses. Thus, both deflections and stresses can be controlled by assigning suitable values to the two gradation parameters. For a sandwich beam with isotropic and homogeneous face sheets and a bi-directionally graded core, the maximum stresses at the interface between the core and the face sheets can be reduced by 40% by suitably tailoring the material properties of the core.

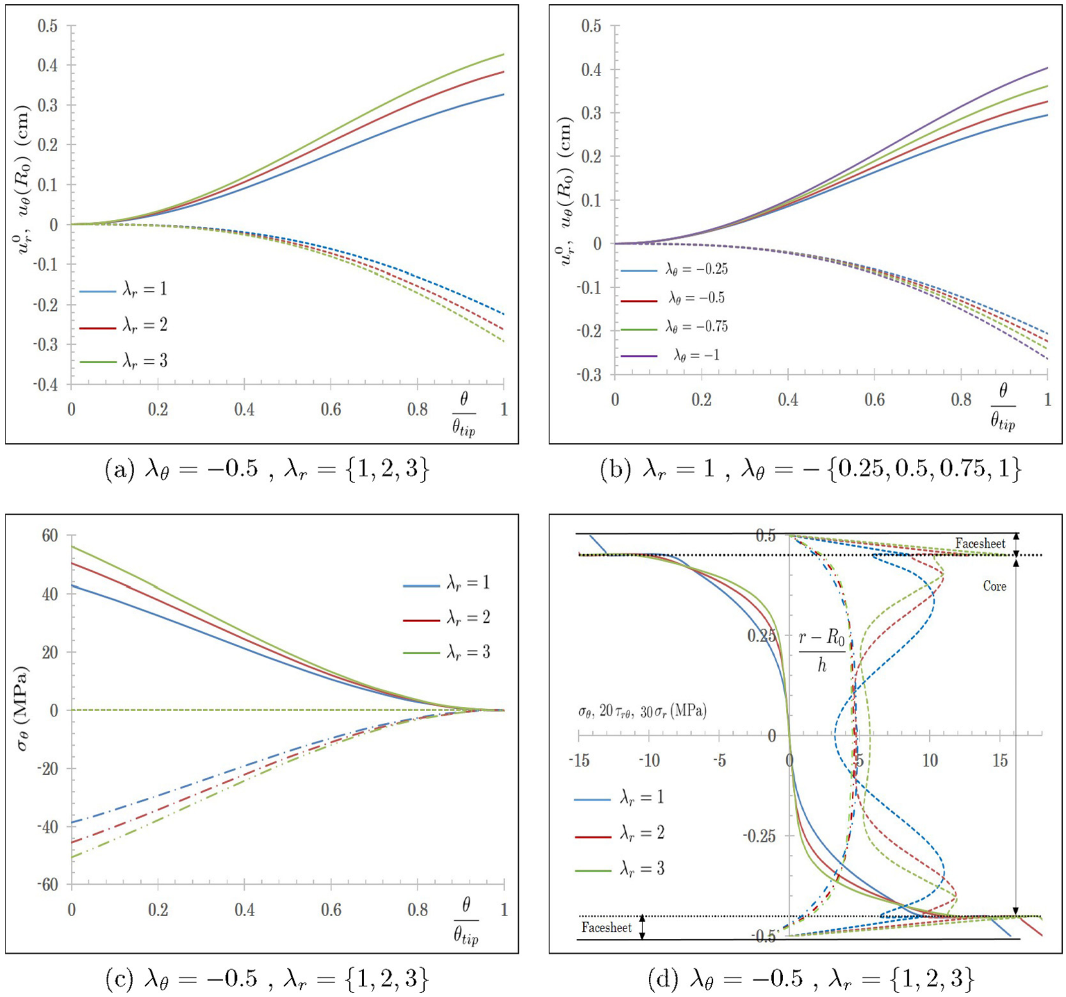

(a) $\lambda_\theta = -0.5$, $\lambda_r = \{1, 2, 3\}$ (b) $\lambda_r = 1$, $\lambda_\theta = -\{0.25, 0.5, 0.75, 1\}$

(c) $\lambda_\theta = -0.5$, $\lambda_r = \{1, 2, 3\}$ (d) $\lambda_\theta = -0.5$, $\lambda_r = \{1, 2, 3\}$

Fig. 17. In a quarter circular cantilever sandwich beam under a uniformly distributed radial force $q^* = 5$ kN/m (a), (b): Centroidal displacements u_r^0 (solid lines) and $u_\theta(R_0, \theta)$ (dashed lines); (c): Bending stress σ_θ along the arc-length at $r = R_0 - \frac{h}{2}$ (solid lines), $r = R_0$ (dashed lines) and $r = R_0 + \frac{h}{2}$ (dash-dot lines), and (d): Bending stress σ_θ (solid lines), shear stress $20\,\tau_{r\theta}$ (dashed lines) and transverse normal stress $30\,\sigma_r$ (dash-dot lines) through the thickness at $\theta = \frac{\pi}{4}$ (dashed lines).

Acknowledgments

RCB's work was partially supported by the US Office of Naval Research Grant N00014-16-1-2309 to Virginia Polytechnic Institute and State University with Dr. Y.D.S. Rajapakse as the program manager. Views expressed in the paper are those of the authors and neither of ONR nor of Virginia Tech. AP would like to thank Mr. Aditya Sabale at IIT Madras and Mr. Arka Chattopadhyay and Mr. Qian Li at Virginia Tech for their help with the finite element simulations. We are indebted to an anonymous reviewer and the editor-in-chief for their suggestions that have improved upon the quality and presentation of the work.

Appendix A

Expressions for the constants $\alpha_i (i = 0, 1 \ldots, 7)$ for a homogeneous material are given below.

$$\alpha_0 = \ln\left(R_0 + \frac{h}{2}\right) - \ln\left(R_0 - \frac{h}{2}\right)$$

$$\alpha_1 = \frac{4\left(3hR_0 + R_0(3R_0 - h)\ln\left(R_0 - \frac{h}{2}\right) - R_0(h + 3R_0)\ln\left(\frac{h}{2} + R_0\right) + h\right)}{h^2}$$

$$\alpha_2 = R_0 \ln(2R_0 - h) - R_0 \ln(h + 2R_0) + h$$

$$\alpha_3 = \frac{h^3 + 3R_0\left(h^2 - 8R_0^2\right)(\ln(2R_0 - h) - \ln(h + 2R_0)) - 24hR_0^2}{3h^2}$$

$$\alpha_4 = -R_0(R_0 \ln(2R_0 - h) - R_0 \ln(h + 2R_0) + h)$$

$$\alpha_5 = \frac{4hR_0 - \left(h^2 - 4R_0^2\right)(\ln(2R_0 - h) - \ln(h + 2R_0))}{h^2}$$

$$\alpha_6 = h$$

$$\alpha_7 = 0$$

Appendix B

Expressions for constants $C_{ir}\,(i = 0, 1, 2, 3), C_{j\theta}\,(j = 0, 1, 2, 3, 4, 5)$ and $C_{k\phi}\,(k = 0, 1, 2)$ used in the expressions for u_r^0, u_θ^0 and ϕ in Section 3.2 are given below.

$$C_{0r} = -\frac{F^*}{bE^*\lambda_\theta e^{\lambda_\theta \theta}\alpha_5\left(\alpha_2^2 - \alpha_0\alpha_4\right)\left(\lambda_\theta^2 + 4\right)}$$

$$C_{1r} = \lambda_\theta(2\alpha_2^2(\nu+1) - 2\alpha_0\alpha_4\nu - 2\alpha_0\alpha_4 + \alpha_4\alpha_5 + \alpha_0\alpha_5R_0^2 + 2\alpha_0\alpha_3\nu R_0 - 2\alpha_1(\nu+1)(\alpha_4+\alpha_2R_0) + 2\alpha_2(\alpha_3(\nu+1)+\alpha_5R_0) + 2\alpha_0\alpha_3R_0)$$

$$C_{2r} = 2(-\alpha_2^2(\nu+1)(\lambda_\theta^2+2) + \alpha_4(\alpha_0(\nu+1)(\lambda_\theta^2+2) + \alpha_1(\nu+1)(\lambda_\theta^2+2) + \alpha_5) + R_0(\alpha_1\alpha_2(\nu+1)(\lambda_\theta^2+2) - \alpha_0\alpha_3(\nu+1)(\lambda_\theta^2+2) + 2\alpha_2\alpha_5) + \alpha_0\alpha_5R_0^2 - \alpha_2\alpha_3(\nu+1)(\lambda_\theta^2+2))$$

$$C_{3r} = -1(\alpha_4(\alpha_5(\lambda_\theta^2+2) + 4\alpha_0(\nu+1) + 4\alpha_1(\nu+1)) - 4\alpha_2^2(\nu+1) - 4\alpha_2\alpha_3(\nu+1) + \alpha_0\alpha_5R_0^2(\lambda_\theta^2+2) + 2R_0(\alpha_5\alpha_2(\lambda_\theta^2+2) + 2\alpha_1\alpha_2(\nu+1) - 2\alpha_0\alpha_3(\nu+1)))$$

$$C_{0\theta} = \frac{F^*}{bE^*\lambda_\theta e^{\lambda_\theta\theta}\alpha_5(\alpha_2^2-\alpha_0\alpha_4)(\lambda_\theta^2+4)(\lambda_\theta^2+1)}$$

$$C_{1\theta} = (\lambda_\theta^2+1)((\alpha_4(\alpha_5(\lambda_\theta^2+2)+4\alpha_0(\nu+1)+4\alpha_1(\nu+1)) - 4\alpha_2^2(\nu+1) - 4\alpha_3\alpha_2(\nu+1)) + R_0(4\alpha_1\alpha_2(\nu+1)(\lambda_\theta^2+1) - 4\alpha_0\alpha_3(\nu+1)(\lambda_\theta^2+1) + \alpha_2\alpha_5(\lambda_\theta^4+2\lambda_\theta^2+4)) - \alpha_0\alpha_5R_0^2(\lambda_\theta^2-2))$$

$$C_{2\theta} = -\frac{1}{\lambda_\theta^2+4}(\lambda_\theta^4+5\lambda_\theta^2+4)(\alpha_4(\alpha_5(\lambda_\theta^2+2)+4\alpha_0(\nu+1)+4\alpha_1(\nu+1)) - 4\alpha_2^2(\nu+1) - 4\alpha_2\alpha_3(\nu+1) + \alpha_0\alpha_5R_0^2(\lambda_\theta^2+2)) + 2R_0(\alpha_5\alpha_2(\lambda_\theta^2+2) + 2\alpha_1\alpha_2(\nu+1) - 2\alpha_0\alpha_3(\nu+1))$$

$$C_{3\theta} = \lambda_\theta((\lambda_\theta^2+1)(-2\alpha_3\alpha_2(\nu+1)(\lambda_\theta^2+3) + \alpha_4(2\alpha_1(\nu+1)(\lambda_\theta^2+3) - 2\alpha_0(\nu+1) + \alpha_5) + 2\alpha_2^2(\nu+1)) - 3\alpha_0\alpha_5R_0^2 + R_0(-2\alpha_1\alpha_2(\nu+1)(\lambda_\theta^2+1) + 2\alpha_0\alpha_3(\nu+1)(\lambda_\theta^2+1)) + \alpha_2\alpha_5(\lambda_\theta^2-2))$$

$$C_{4\theta} = \frac{\lambda_\theta}{\lambda_\theta^2+4}(\lambda_\theta^4+5\lambda_\theta^2+4)(2\alpha_2^2(\nu+1) + \alpha_4(-2\alpha_0(\nu+1) - 2\alpha_1(\nu+1) + \alpha_5) + 2\alpha_2\alpha_3(\nu+1) + \alpha_0\alpha_5R_0^2 + 2R_0(\alpha_1\alpha_2(-\nu-1) + \alpha_0\alpha_3(\nu+1) + \alpha_5\alpha_2))$$

$$C_{5\theta} = R_0\alpha_5\lambda_\theta^2(\alpha_2+\alpha_0R_0)(\lambda_\theta^2+4)$$

$$C_{0\phi} = \frac{F^*}{bE^*e^{\lambda_\theta\theta}\alpha_5(\alpha_2^2-\alpha_0\alpha_4)(\lambda_\theta^2+1)}$$

$$C_{1\phi} = \alpha_5\lambda_\theta(\alpha_2+\alpha_0R_0)$$

$$C_{2\phi} = 2\alpha_1\alpha_2(\nu+1)(\lambda_\theta^2+1) + \alpha_2\alpha_5 - \alpha_0(2\alpha_3(\nu+1)(\lambda_\theta^2+1) - \alpha_5R_0)$$

References

[1] Suresh S, Mortensen A. Fundamentals of functionally graded materials: processing and thermomechanical behaviour of graded metals and metal-ceramic composites. 1998. London: IOM Communications Ltd; 2011.
[2] Christensen R. Mechanics of composite materials. Massachusetts, U.S. A: Courier Corporation; 2012.
[3] Wetherhold R, Seelman S, Wang J. The use of functionally graded materials to eliminate or control thermal deformation. Compos Sci Technol 1996;56(9):1099–104.
[4] Chakraborty A, Gopalakrishnan S, Reddy J. A new beam finite element for the analysis of functionally graded materials. Int J Mech Sci 2003;45(3):519–39.
[5] Timoshenko SP. X. On the transverse vibrations of bars of uniform cross-section. London Edinburgh Dublin Philos Mag J Sci 1922;43(253):125–31.
[6] Oldfather W, Ellis C, Brown DM. Leonhard Euler's elastic curves. Isis 1933;20(1):72–160.
[7] Wang C, Reddy JN, Lee K. Shear deformable beams and plates: relationships with classical solutions. Elsevier; 2000.
[8] Carrera E, Giunta G, Petrolo M. Beam structures: classical and advanced theories. John Wiley & Sons; 2011.
[9] Nie G, Batra R. Exact solutions and material tailoring for functionally graded hollow circular cylinders. J Elast 2010;99(2):179–201.
[10] Venkataraman S, Sankar B. Elasticity solution for stresses in a sandwich beam with functionally graded core. AIAA J 2003;41(12):2501–5.
[11] Ding H, Huang D, Chen W. Elasticity solutions for plane anisotropic functionally graded beams. Int J Solids Struct 2007;44(1):176–96.
[12] Li X-F. A unified approach for analyzing static and dynamic behaviors of functionally graded Timoshenko and Euler-Bernoulli beams. J Sound Vib 2008;318(4):1210–29.
[13] Sina S, Navazi H, Haddadpour H. An analytical method for free vibration analysis of functionally graded beams. Mater Des 2009;30(3):741–7.
[14] Giunta G, Belouettar S, Carrera E. Analysis of FGM beams by means of classical and advanced theories. Mech Adv Mater Struct 2010;17(8):622–35.
[15] Bîrsan M, Altenbach H, Sadowski T, Eremeyev V, Pietras D. Deformation analysis of functionally graded beams by the direct approach. Compos Part B: Eng 2012;43(3):1315–28.
[16] Yoon K, Lee P-S, Kim D-N. Geometrically nonlinear finite element analysis of functionally graded 3D beams considering warping effects. Compos Struct 2015;132:1231–47.
[17] Nguyen T, Kim N-I, Lee J. Analysis of thin-walled open-section beams with functionally graded materials. Compos Struct 2016;138:75–83.
[18] Wu L, Wang Q, Elishakoff I. Semi-inverse method for axially functionally graded beams with an anti-symmetric vibration mode. J Sound Vib 2005;284(3):1190–202.
[19] Huang Y, Li X-F. A new approach for free vibration of axially functionally graded beams with non-uniform cross-section. J Sound Vib 2010;329(11):2291–303.
[20] Shahba A, Attarnejad R, Marvi MT, Hajilar S. Free vibration and stability analysis of axially functionally graded tapered Timoshenko beams with classical and non-classical boundary conditions. Compos Part B: Eng 2011;42(4):801–8.
[21] Sarkar K, Ganguli R. Closed-form solutions for axially functionally graded Timoshenko beams having uniform cross-section and fixed-fixed boundary condition. Compos Part B: Eng 2014;58:361–70.
[22] Lü C, Chen W, Xu R, Lim CW. Semi-analytical elasticity solutions for bi-directional functionally graded beams. Int J Solids Struct 2008;45(1):258–75.
[23] Qian L, Batra R. Design of bidirectional functionally graded plate for optimal natural frequencies. J Sound Vib 2005;280(1):415–24.
[24] Goupee AJ, Vel SS. Optimization of natural frequencies of bidirectional functionally graded beams. Struct Multi Optim 2006;32(6):473–84.
[25] Şimşek M. Bi-directional functionally graded materials (BDFGMs) for free and forced vibration of Timoshenko beams with various boundary conditions. Compos Struct 2015;133:968–78.
[26] Wang Z, Wang X, Xu G, Cheng S, Zeng T. Free vibration of two-directional functionally graded beams. Compos Struct 2016;135:191–8.
[27] Malekzadeh P, Haghighi MG, Atashi M. Out-of-plane free vibration of functionally graded circular curved beams in thermal environment. Compos Struct 2010;92(2):541–52.
[28] Kurtaran H. Large displacement static and transient analysis of functionally graded deep curved beams with generalized differential quadrature method. Compos Struct 2015;131:821–31.
[29] Tufekci E, Eroglu U, Aya SA. Exact solution for in-plane static problems of circular beams made of functionally graded materials. Mech Based Des Struct Mach 2016;44(4):476–94. http://dx.doi.org/10.1080/15397734.2015.1121398.
[30] Rastgo A, Shafie H, Allahverdizadeh A. Instability of curved beams made of functionally graded material under thermal loading. Int J Mech Mater Des 2005;2(1–2):117–28.
[31] Shafiee H, Naei M, Eslami M. In-plane and out-of-plane buckling of arches made of FGM. Int J Mech Sci 2006;48(8):907–15.
[32] Yousefi A, Rastgoo A. Free vibration of functionally graded spatial curved beams. Compos Struct 2011;93(11):3048–56.
[33] Fereidoon A, Andalib M, Hemmatian H. Bending analysis of curved sandwich beams with functionally graded core. Mech Adv Mater Struct 2015;22(7):564–77. http://dx.doi.org/10.1080/15376494.2013.828815.
[34] Eroglu U. In-plane free vibrations of circular beams made of functionally graded material in thermal environment: Beam theory approach. Compos Struct 2015;122:217–28.
[35] Kardomateas G. Bending of a cylindrically orthotropic curved beam with linearly distributed elastic constants. Q J Mech Appl Mech 1990;43(pt 1):43–55.
[36] Filipich C, Piovan M. The dynamics of thick curved beams constructed with functionally graded materials. Mech Res Commun 2010;37(6):565–70.
[37] Piovan M, Domini S, Ramirez J. In-plane and out-of-plane dynamics and buckling of functionally graded circular curved beams. Compos Struct 2012;94(11):3194–206.

[38] Eroglu U. Large deflection analysis of planar curved beams made of functionally graded materials using variational iterational method. Compos Struct 2016;136:204–16.
[39] Dryden J. Bending of inhomogeneous curved bars. Int J Solids Struct 2007;44:4158–66.
[40] Wang M, Liu Y. Elasticity solutions for orthotropic functionally graded curved beams. Eur J Mech-A/Solids 2013;37:8–16.
[41] Lim C, Yang Q, Lü C. Two-dimensional elasticity solutions for temperature-dependent in-plane vibration of FGM circular arches. Compos Struct 2009;90(3):323–9.
[42] Malekzadeh P. Two-dimensional in-plane free vibrations of functionally graded circular arches with temperature-dependent properties. Compos Struct 2009;91(1):38–47.
[43] Pydah A, Sabale A. Static analysis of bi-directional functionally graded curved beams. Compos Struct 2017;160:867–76. ISSN 0263-8223.
[44] Pydah A, Sabale A, A shear deformation-based model for the analysis of thick bi-directional functionally graded circular beams (under review), Compos Part B: Eng.
[45] Lutz MP, Zimmerman RW. Thermal stresses and effective thermal expansion coefficient of a functionally gradient sphere. J Therm Stresses 1996;19(1):39–54.
[46] Martínez-Pañeda E, Gallego R. Numerical analysis of quasi-static fracture in functionally graded materials. Int J Mech Mater Des 2015;11(4):405–24.
[47] Love AEH. A treatise on the mathematical theory of elasticity, vol. 1. Cambridge University Press; 2013.
[48] Batra R, Xiao J. Analysis of post-buckling and delamination in laminated composite St. Venant-Kirchhoff beams using CZM and layer-wise TSNDT. Compos Struct 2013;105:369–84.
[49] Batra R, Xiao J. Finite deformations of full sine-wave St.-Venant beam due to tangential and normal distributed loads using nonlinear TSNDT. Meccanica 2015;50(2):355–65.
[50] Toupin R. Saint-Venant's Principle. Arch Rational Mech Anal 1965;18:83–96.
[51] Batra R. Saint-Venant's Principle for a helical spring. J Appl Mech 1978;45:297–301.